Progress In Electromagnetics Research, Vol. 149, 55–67, 2014

Chiral Metamaterial Based Multifunctional Sensor Applications

Muharrem Karaaslan and Mehmet Bakir*

Abstract—In this work, sensor abilities of a chiral metamaterial based on split ring resonators with double splits (SRDS) are demonstrated both theoretically and experimentally in X band range. This study is based on transmission measurements and simulations monitoring the resonance frequency changes with respect to the thickness of the sensing layer and permittivity values. Experimental and simulated results show that the resonance frequency of the chiral metamaterial based SRDS sensor is linearly related to the permittivity and the thickness of the sensor layer which creates a suitable approach for sensing environment and organic parameters. When the sensor layer filled with the related material, changes in the tissue temperature, sand humidity and calcium chloride density lead to resonance frequency changes. The physical mechanisms are explained by using both equivalent circuit model and the fundamental sensitivity theorem of chiral sensors. This is the first study investigating a sensing mechanism based on the chiral metamaterials in X band range.

1. INTRODUCTION

Researchers produce an artificial micro-sized medium such as left-handed materials (LHMs) by using micro- and nano-fabrication techniques in order to manage electromagnetic (EM) waves in controllable way. LHMs, a subset of the metamaterials, are based on arrays of classical plasmonic resonators which have been designed to acquire simultaneous negative permittivity and negative permeability values providing negative refraction. The LHMs are man-made materials showing extraordinary characteristics that cannot be found in nature [1, 2]. In this case, a split-ring resonator (SRR) structure which has been used more than a decade in order to produce magnetic response in various types of metamaterials from microwave to optical region is artificially produced. The SRR type metamaterials can be used to create strong magnetic coupling among the EM fields which cannot be available in conventional methods. There are some studies realizing magnetic resonances by using different SRR configurations in literature [3–12]. SRR topology consists of more than one coupled SRR unit cell. This feature provides mutual inductance and capacitance effects at the resonance frequency according to their positions [13].

In a chiral medium, an electric field causes magnetic polarization, and a magnetic field induces an electrical polarization which is defined as magneto-electric coupling [14]. When a metamaterial involves chiral inclusions, it can be considered as a chiral metamaterial meaning that the effective chirality admittance (ζ) is non-zero. Wave propagation properties in a chiral metamaterials demonstrate that the negative refraction can be obtained with a strong chirality without requiring negative ε or μ [15, 16].

Metamaterial studies have reached an advanced level due to a continual progress in design and fabrication of metamaterials on micro- and nano-scale levels. Due to the relation between metamaterial science and sensing technology, new scientific and technological applications have been developed in this particular field. Furthermore, considerable advances have been realized on the metamaterial based sensors which lead to detecting information of a substance and a situation. The metamaterial based sensors which generally have SRRs are developed for the observation of environmental parameters

Received 1 July 2014, Accepted 14 August 2014, Scheduled 28 August 2014

* Corresponding author: Mehmet Bakir (mehmet.bak@gmail.com).
The authors are with the Department of Electrical and Electronics Engineering, Mustafa Kemal University, Iskenderun, Hatay 31200, Turkey.

because of their resonance frequencies since the environmental parameters change the resonance frequencies.

Sensors have to meet some requirements in order to work effectively. For example, they must have a loss factor as low as possible to prevent substrate absorption. Hence, we have chosen a polyester laminate GML 1000 type substrate material with a loss tangent of 0.004. Secondly, the sensors must give a measurable signal according to the changes in the parameters. The third one is the linearity meaning that the sensor must shift the resonance frequency sharply or smoothly according to the quantity of the changes in the observed parameter. The fourth one is the sensor sensitivity. If the sensitivity is high, related shifts can easily be observed from the network analyzer.

These suggested requirements are considered and realized in this study to obtain a new sensor based on a chiral metamaterial designed by square-ring with double splits (SRDS) which have high efficiency and gain. There are many advantages of the proposed study compared to the metamaterial based sensor studies in literature. The reason is that this study takes advantages of chiral metamaterials which have some unusual EM features such as optical activity, negative refraction, etc. [17, 18]. The suggested SRDS-shaped resonator based on chiral metamaterial introduces an alternative and new approach to the sensor applications. These advantages are discussed and verified both experimentally and numerically. Theoretical and experimental analysis of the proposed sensor application is realized in detail.

The organization of this study is as follows. In Section 2, the design of the chiral unit cell is explained. In Section 3, an experiment and a simulation of the chiral MTMs based on discontinuous bilayer cross-wires structure are proposed. The experiment and simulation methods are introduced. In Section 4, a chiral metamaterial based pressure sensor application together with the idea of using the resonance frequency change in a sensor is substantiated. In Section 5, generalization of the idea and the design of chiral structures are presented. In Section 6, a chiral metamaterial based sensor application is demonstrated. Finally, summary and conclusions are given at the end of the paper.

2. DESIGN OF THE CHIRAL UNIT CELL

The SRDS-sensor design involves a sensor layer and a structure. Sensor layer is placed between two chiral metamaterial based sensor structures in order to sense changes in pressure, tissue temperature, sand humidity and calcium chloride density as multi-functional. There is a 90-degree difference between the front and back sides of the SRDS structures as shown in Fig. 1(a). Each SRDS structure is produced from the same material in the same size and the same dimensions in order to keep chiral metamaterial components constant. The most important parameter of the SRDS sensor is resonance frequency. Generic resonance frequency of split-ring resonators can be considered as a RLC resonance circuit that can be defined as $\frac{1}{\sqrt{LC}}$. Inductance and capacitance parameters of the SRDS must include self and mutual terms according to the design of metamaterial and thickness of the substrate [19, 20]. Each

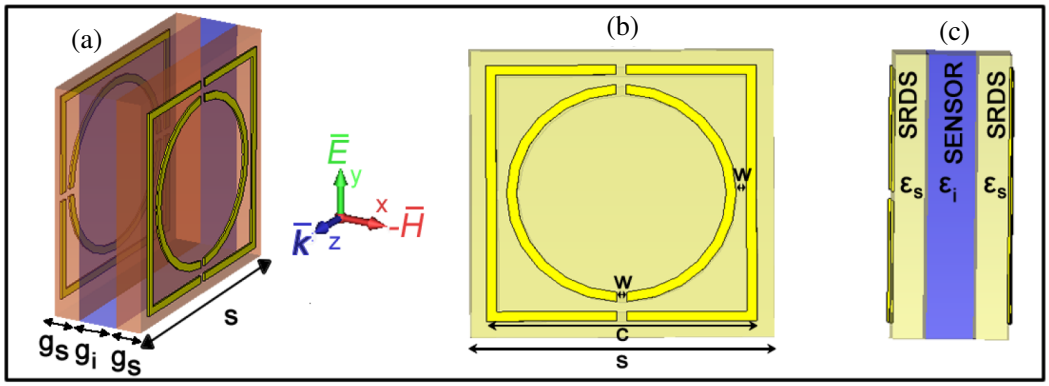

Figure 1. The designed SRDS based metamaterial sensor, (a) a 3D-perspective view, (b) unit cell with dimensions, (c) a side view.

SRDS structure is placed opposite sides of the unit cell to create powerful coupling. We designed the SRDS structure not only to meet the sensor requirements explained before but also to increase sensitivity in different sensing areas for physical and biological applications. In this study, the substrate and metal thickness of SRDS structures are kept fixed to monitor the changes between the sensor layer permittivity (ε_i) and the resonance frequency. The Sensor layer is going to be used for sensing the changes of the environmental parameters. In this study, the effects of the changes in thickness of the sensing layer (g_i) and dielectric constant of the sensing layer (ε_i) have been used effectively for sensing environmental parameters as to be demonstrated in the rest of the paper.

We have two identical SRDS structures which are placed in a unit cell with 90° difference in order to achieve asymmetry. This asymmetry of the structure provides both chirality and rotated electromagnetic wave composed of right- and left-hand circularly polarized parts. Hence, it will contribute stronger sensing of sandwiched dielectric layer with respect to the metamaterial based sensors [21]. The SRDS structures are printed on a polyester laminate GML 1000 type substrate material due to its low loss characteristics. The GML 1000 material has dielectric constant of $\varepsilon_s = 3.05$, loss tangent of $\zeta = 0.004$ at 10 GHz with a substrate thickness of $g_s = 0.5$ mm. One side of GML 1000 is coated with SRDS inclusions to provide surface current. Copper thickness and conductivity are 0.035 mm and $\sigma_{cu} = 58 \times 10^6$ S/m, respectively. SRDS unit cell has the following dimensions: substrate with width $s = 4.5$ mm, copper length $c = 4$ mm, gap between the square and circle strip $w = 0.15$ mm as shown in Fig. 1(b). These parameters are kept constant during the simulations and the experiments for all suggested sensor types. The SRDS structures are separated from each other by a sensing layer. The sensing layer is defined with a variable thickness value of g_i and a dielectric constant of ε_i to determine the sensitivity of the structure with respect to the changes in density and pressure as shown in Fig. 1(c).

3. SIMULATION AND EXPERIMENTAL SETUP

The proposed SRDS sensor can be used to sense different parameters according to the changes in dielectric constant and thickness of sensing layer which are investigated numerically and experimentally in the following sections. The fabricated SRDS structure is given in Fig. 2(a). We investigate the performance of the SRDS based chiral metamaterial sensor as a density and a pressure sensors both numerically and experimentally. In addition, humidity, temperature and density sensors are also investigated numerically as can be seen in the following sections.

In the experimental setup, two-port rectangular waveguide has been used for sensing applications between 8–12 GHz as shown in Fig. 2(b). Two ports are connected to the vector network analyzer (VNA) by using two waveguide adapters. Complex values of reflection and transmission parameters (S-parameters) have been both simulated and measured for the SRDS sensor via finite integration technique based simulator (CST Microwave Studio) and the network analyzer, respectively. The

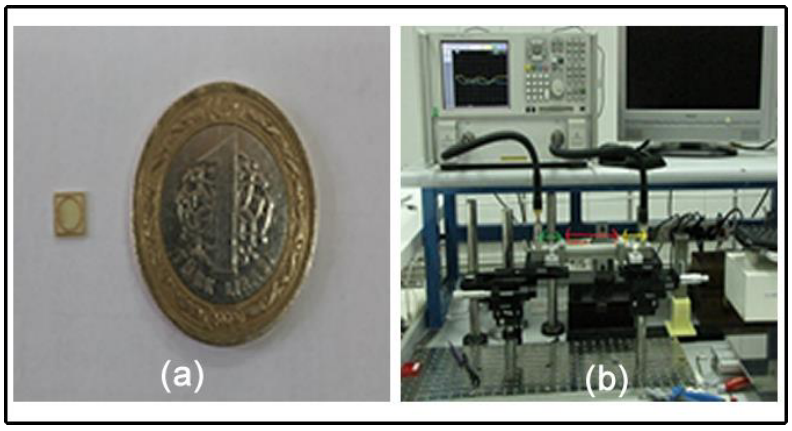

Figure 2. (a) An image of front side of the SRDS sample fabricated in microwave scale, (b) measurement setup of the sample.

analyzer is calibrated before SRDS measurement accordingly to achieve accurate results. The SRDS sensor structure is placed at the bottom of the calibrated waveguide to provide appropriate interaction. Fabricated SRDS sensor structure is fixed in the unit cell by a sample holder to realize accurate measurement. Sample holder's permittivity and permeability values are very close to the air ($\mu_r \cong 1,\ \varepsilon_r \cong 1$) to prevent undesired interaction. As a result, the sensor holder does not influence measurements by undesirable reflection or absorptions. TE_{10} waveguide mode has been used for the experiments, hence the resonance of the overall structure is provided due to the propagation of magnetic field component of the incident wave through the center of SRDS unit cell.

CST Microwave studio has been used for the numerical simulations described in this study. Conducting wall type boundary conditions are applied in X and Y directions while open boundary condition is applied in Z direction in order to match simulation and experimental results. During simulation, port 1 and port 2 dimensions are adjusted according to the waveguide volume and dimensions in order to achieve accurate simulations. After necessary adjustments, both numerical and experimental results are matched. CST microwave studio efficiently simulates two-dimensional SRDS structure in xy-plane. Because of the larger dimensions of the X band waveguide, SRDS structure is quite small but highly effective in this study. The SRDS unit cell behaves as periodically arranged two-dimensional SRDS arrays due to the assignment of the conducting walls in x-y planes, since conducting wall boundaries provide imaging effect on the unit cell. Consequently, coupling between the unit cells of this array can also be neglected because of the mirror behavior of waveguide walls and electromagnetic characteristics of unit cell array getting closer to a periodic array of a unit cell. Measurement results of a single cell and in the waveguide and measurement results that can be realized in free space for sensor which has more than a single cell would be similar to each other. This measurement technique for a unit cell in a waveguide as an array is used in many studies of metamaterials especially in the cases where an anechoic chamber is not present. Beside this, the agreement of simulation and measurement results is also an indicator showing that the simulation setup is correct. Numerical setup and SRDS test diagram are shown in Fig. 3, respectively.

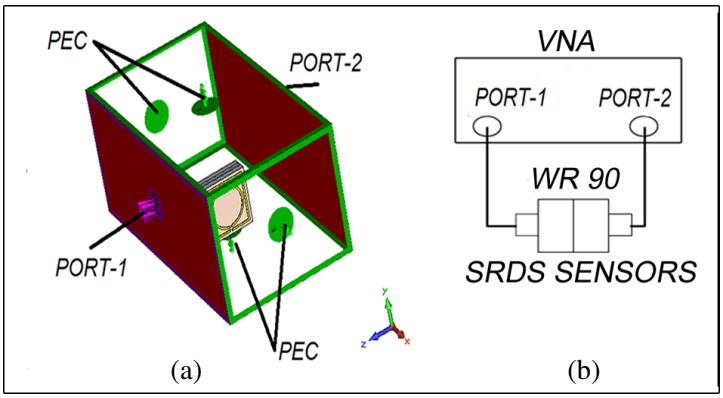

Figure 3. Structure based on SRDS, (a) numerical setup, (b) a schematic view of the experimental setup, respectively.

Before the investigation of the SRDS structure as a sensor, the electromagnetic properties and physical mechanism are analyzed. The main uncommon characteristic of the SRDS based structure except for better sensing properties and linearity with respect to the studies in literature [20] is the optical activity as can be seen below. SRDS inclusions are asymmetrically placed in the front and back sides of GML 1000 type substrates. It can be concluded that the change of the dielectric constant of the sandwiched dielectric layer between SRDS inclusions as a chiral metamaterial is much more sensitive than MTM based sensors. It can be decided by comparing the results of this study and metamaterial based sensor studies [20–23]. The physical mechanism of the SRDS based chiral structure and sensing layer can easily be explained by the help of the interaction of asymmetric waves and the sensing layer. The electric field coupling with localized surface current distributions is concentrated

along SRDS inclusions. The sensing material between SRDS inclusions interact more strongly with the optically activated wave with respect to the metamaterials with lack of asymmetry. It can be concluded that the sensing layer adjacent to the SRDS inclusions will strongly affect the resonance frequency of the sensing layer. This mechanism is the fundamental of sensitivity of chiral sensors [24–27]. The shift of the resonance frequency with respect to the dielectric layer between chiral inclusions can be defined by the following equation [28];

$$\Delta\lambda = s\Delta n \left[1 - e^{\left(\frac{-2d}{1_d}\right)}\right] \tag{1}$$

where s defines the sensitivity constant in the change of the local refractive index, and n, d, and 1_d represent difference of effective refractive index due to the dielectric layer, thickness of dielectric layer and vanishing distance of local fields. The condition of estimation for this equation is the presence of chirality. Hence, we investigate the chirality admittance (κ) of the SRDS based structure by the equation [29];

$$\mathrm{Re}(\kappa) = \frac{\phi_+ - \phi_- + 2m\pi}{2k_0 d} \tag{2}$$

where ϕ_+ and ϕ_- represent the polarization angle rotation of right and left circular components of EM wave through SRDS inclusions. The parameter m is an integer and determined by the condition of $-\pi < \phi_\pm - \phi_- + 2m\pi < \pi$ where k_0 and d denote free-space wave number and thickness of overall structure, respectively. The simulation is realized with the RT 5870 material placed as a sensing layer (RT 5870 $\varepsilon_s = 2.33$, $g_i = 0.76$ mm). Both the resonance frequency and chirality plots are shown below. It is shown that the chirality admittance of SRDS based chiral structure is around 0.87 at the resonance frequency (9.87 GHz). Therefore, it can be emphasized that the resonance shifts can be explained by the chirality properties and the effects of changes in the sandwiched layer. Chirality admittance value is shown in Fig. 4 for RT5870 dielectric material.

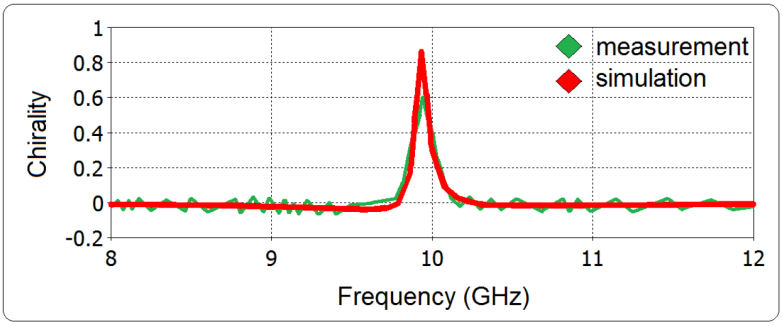

Figure 4. Simulated and measured chirality admittance values based on SRDS for RT5870 dielectric material.

4. PRESSURE SENSOR APPLICATION OF THE CHIRAL METAMATERIAL

In the SRDS based pressure sensor application, sensor layer is composed of air (i.e., $\varepsilon_i = 1$). Whereas, one of the SRDS structure is fixed, the other one can move along only x axis to represent the effect of pressure which is applied to the one surface of overall structure. All the dimensions and other properties of the SRDS structure are kept constant. Relationship between the change on the thickness of sensor layer and resonance frequency of the SRDS sensor can be associated according to the pressure level. To prove that, we have numerically simulated and experimentally tested five different values (0.40, 0.80, 1.20, 1.60 and 2.00 mm), of g_i as the sensing layer as shown in Figs. 5(a) and 5(b), respectively. To verify the simulation results of pressure sensor topology, the proposed structure is both fabricated and measured. While the pressure on the sensing layer is reduced from 0.4 mm to 2 mm, both mutual inductance and capacitance between SRDR structures on two surfaces also decrease due to the distance dependency and resonance frequency shifts upward from 9.8 GHz to 10.4 GHz (dB magnitude of $|S_{21}|$ versus frequency curves) as shown in Fig. 5(a). Variation between simulated and experimental results

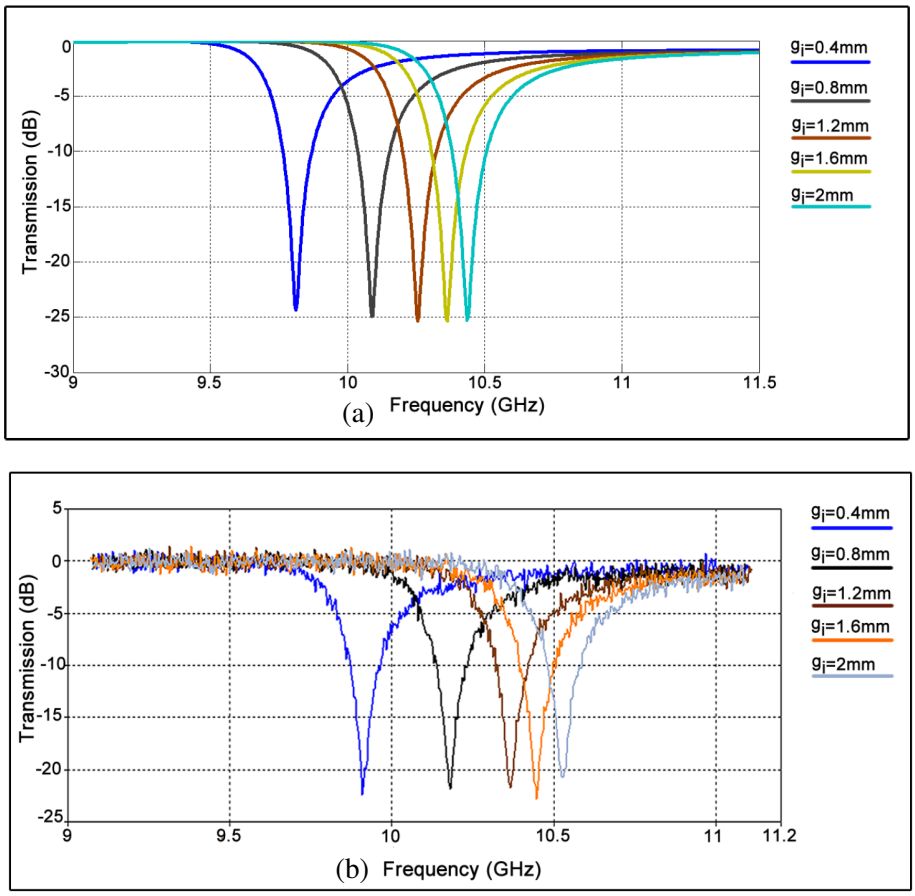

Figure 5. Transmission curves of the SRDS based pressure sensor model according to the different layer thickness. (a) Simulated and (b) measured results, respectively. ($g_s = 0.5$, $\varepsilon_i = 1$, $\varepsilon_s = 3.05$).

is around 1% for the center frequency of 10 GHz as shown in Fig. 5(b). The transmission values for all pressure levels are constant and around −25 dB. These are the main advantages of the proposed SRDS sensor on the other MTM sensor studies. In particular, the transmission values are around −13 dB and not constant in one of those studies [20]. The effect of the thickness of the chiral layer on wavelength shift can be determined from Eq. (1). Whereas the dielectric material thickness between SRDS inclusions is increasing, resonance wavelength shifts upward, meaning that the resonance frequency shifts downward. It is observed that the numerical results are in a good agreement with the experimental ones. Very small difference is observed which could be caused by the production or calibration techniques.

5. TEMPERATURE, DENSITY AND HUMIDITY APPLICATION OF THE CHIRAL METAMATERIAL

Many other sensing applications can be realized by using SRDS based chiral MTM sensor such as temperature, humidity and density sensing. In order to measure humidity, density or temperature, sensor layer dimensions are kept fixed, and sensor layer is filled with different materials having variable relative permittivity (ε_i) to sense the changes in temperature, humidity and density. In order to justify sensor applications, four different materials which have different dielectric constants are used in sensor layer. Numerical and experimental studies are realized by Roger RT5870 ($\varepsilon_i = 2.33$) AD25N ($\varepsilon_i = 3.38$), AD 450 ($\varepsilon_i = 4.50$) and Aluminum substrate ($\varepsilon_i = 9.9$) as shown in Figs. 6(a) and 6(b), in order. Experimental and simulated results are similar for the SRDS based sensor layer with a thickness of $g_i = 0.76$ mm as shown in Figs. 6(a) and 6(b). The maximum slide of resonance frequency between

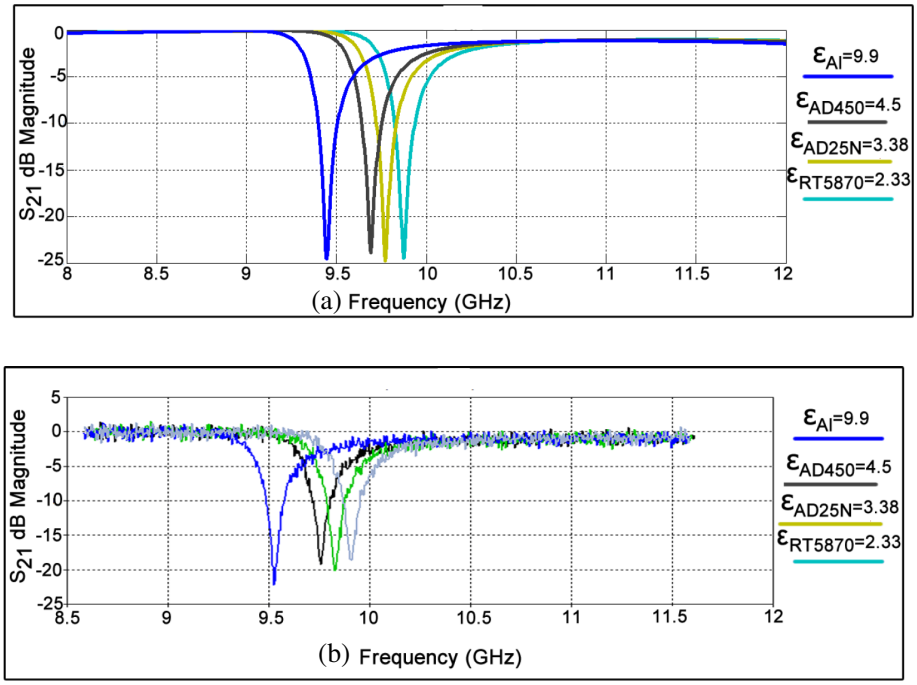

Figure 6. Transmission curves of the SRDS based pressure sensor model according to the different layer dielectric constant. (a) Simulated and (b) measured results, respectively. (GML 1000 $\varepsilon_s = 3.05$, $g_s = 0.508\,\text{mm}$).

simulation and measurement is only around 1% for the center frequency of 9.5 GHz. When the relative permittivity of the sensing layer shifts from 2.33 to 9.9, SRDS resonance frequency shifts from 9.52 GHz to 9.92 GHz. The main advantages of the proposed structure is the stable value of the transmission constant and the lower value of transmission with respect to the topologies in literature for sensing [20–23].

In this study, self-inductance (L_{self}) of each SRDS is constant since it is only affected by the circulated metallic path dimensions and wavelength of the incident EM wave. The variation of permittivity does not affect L_{self} of the SRDS because of not having magnetic properties. Mutual inductance between rotated SRDS does not change due to the constant dimensions of the substrate thickness and the sensor layer thickness in this part. Beside this, there is no factor resulting in a change of the individual mutual inductance.

The self-capacitance (C_{self}) of the SRDS is related to gap capacitances and especially with the capacitances between outer square and inner circular rings. The interaction between relative permittivity of sensing layer and C_{self} is directly proportional as can be concluded from electric field distribution. Both the gap capacitance and the capacitance between the rings increase depending on the dielectric constant of the sensing layer.Electric field distribution and surface current distribution of SRDS inclusions are given in Fig. 7. It can be seen that the electric field is concentrated on the gap of resonators and the surface current is highly concentrated on the metal inclusions.

It can be concluded that ε_{eff}(sub) which directly affects C_{sefl} of individual SRDS increases depending on the substrate thickness and substrate permittivity. It means that C_{self} of the rotated SRDS are related with both thickness and relative permittivity of each sandwiched layers ε_i, ε_s, g_i, and g_s. Hence, the mutual capacitance which denotes the interaction of rotated SRDS can be represented by equivalent model of series capacitance composed of two different base capacitance for ε_s and one sandwiched sensing layer;

$$\frac{1}{C_{mut}} = \frac{1}{C_{b_1}} + \frac{1}{C_{int}} + \frac{1}{C_{b_2}}, \quad C_b = \frac{\varepsilon_{s(a)}}{g_s}, \quad C_{int} = \frac{\varepsilon_{int(A)}}{g_i} \tag{3}$$

"A" denotes the metal part area of SRDR. As can be concluded from the equation, C_{mut} changes

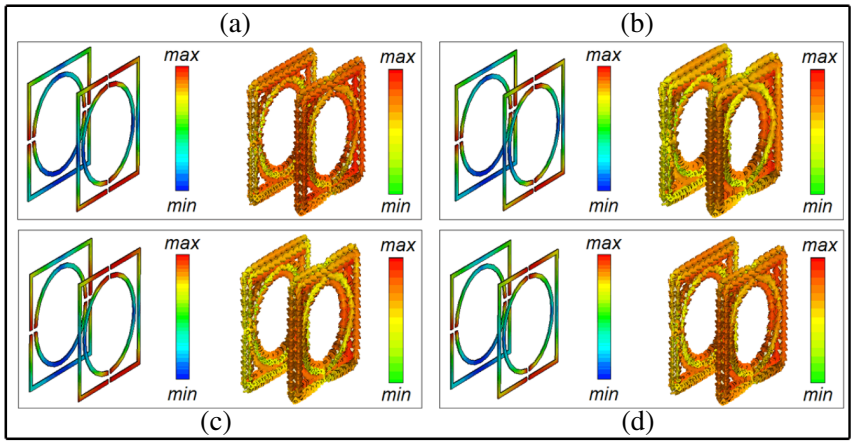

Figure 7. Electric field and surface current distributions, (a) at the resonance frequency of 9.87 GHz for RT 5870 dielectric material, (b) at the resonance frequency of 9.77 GHz for AD 25N dielectric material, (c) at the resonance frequency of 9.69 GHz for AD 450 dielectric material, (d) at the resonance frequency of 9.44 GHz for alumina dielectric material, respectively.

depending on C_{int} in the case of variation of the permittivity of the sandwiched sensing layer even when all other variables are kept constant. It means that both C_{self} and C_{mut} increase with the sensing layer permittivity. Beside this, C_{mut} can also be changed by varying the values of g_s and g_i. Variation of g_s also changes the unequal values of C_b and differs both the interaction of the rotated SRDSs which results in alteration of optical activity and value of C_{self}. Hence, it must be concluded that C_{self} of the rotated SRDS inclusions have deeper effect on mutual capacitance. As a result, the resonance frequency of the SRDS based chiral sensor is inversely proportional with total capacitance of sensing system, while C_{tot} is directly related with dielectric constant of the sandwiched layer. The shift of the resonance frequency can also be explained by chiral sensor definition. While permittivity of the sensing layer increases, refractive index also increases, and resonance frequency decreases with the inverse of wavelength (Eq. (1)).

6. OTHER SENSOR APPLICATIONS

Moisture sensor, density sensor and temperature sensor applications are investigated to emphasize the usage of the proposed chiral sensor model in this part.

6.1. SRDS Based Moisture Sensor

Sample water content (WC) investigation is given in this section for the suggested chiral sensor model. Sensor layer is accepted to be filled by sand. In order to simulate water content measurement, we must know the dielectric constant of material which fills the sensor layer. For this reason, we used percentage water content and complex relative permittivity data taken from [30], and dielectric constant of sensor layer is defined as $\varepsilon_i = \varepsilon_r' - j\varepsilon_r''$. The numerical data are seen in the inset of Fig. 8 with loss tangent values ($\tan\delta = \varepsilon'/\varepsilon''$). Thickness of the sensor layer is fixed to 0.76 mm during simulation in order to neglect thickness changes of the sensor layer. After obtaining the required data, reflection and transmission coefficients (S parameters) for two-port structures are calculated by using CST Microwave Studio for our SRDS humidity sensor model. Variation of resonance frequency versus moisture content is shown in Fig. 8. It is clear that whereas moisture percentage is changing between 0–17 percent according to 10 water contents listed in the inset, resonance frequency is decreased inversely from 9.712 to 9.152 GHz. The change of resonance frequency is nearly linear with a slope of 33 MHz per unit water content. According to the table in Fig. 8, water content in the sand affects resonance frequency nearly %0.2. This increment can be easily observed with all network analyzers. Hence the proposed SRDS based chiral sensor is suitable for measuring the variations of moisture with excellent sensitivity. The suggested

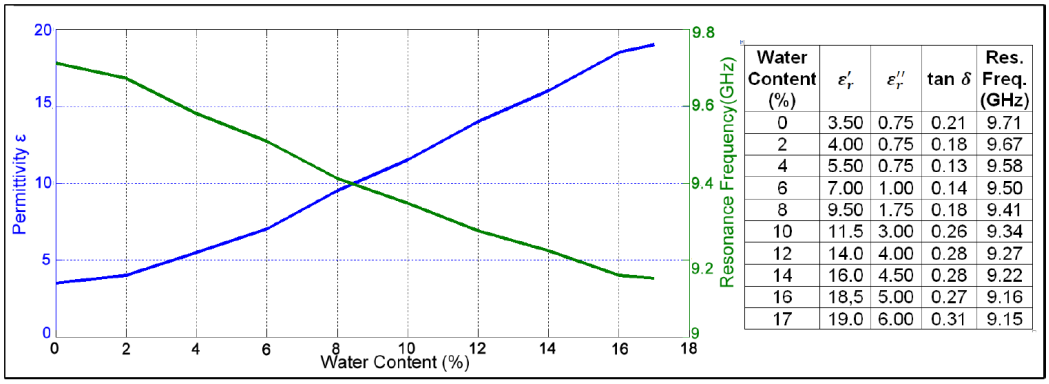

Water Content (%)	ε_r'	ε_r''	tan δ	Res. Freq. (GHz)
0	3.50	0.75	0.21	9.71
2	4.00	0.75	0.18	9.67
4	5.50	0.75	0.13	9.58
6	7.00	1.00	0.14	9.50
8	9.50	1.75	0.18	9.41
10	11.5	3.00	0.26	9.34
12	14.0	4.00	0.28	9.27
14	16.0	4.50	0.28	9.22
16	18,5	5.00	0.27	9.16
17	19.0	6.00	0.31	9.15

Figure 8. Variations of resonance frequency of the SRDS based sensor according to different water contents.

moisture sensor is much more realistic with respect to the MTM moisture sensors in literature since the range of water content of tested materials in the literature is much greater, and the step points are not regular [20]. The distortion of linearity is directly related with the nonlinear change of permittivity of the content. The changes of the resonance frequency of overall sensing mechanism can also be described by both equivalent circuit model and chiral MTM based sensor topology. According to the chiral MTM sensor topology, the increment of the dielectric constant of sensing layer increases the refractive index of the sandwiched layer and thusshifts the wavelength. As a result, the resonance frequency shifts to the upper frequencies. In accordance with equivalent circuit approach, overall capacitance of the circuit is directly proportional with dielectric constant of the sensing layer, and the increment of overall capacitance reduces the resonance frequency.

6.2. SRDS Based Density Sensor

Effects of calcium chloride density changes in the silica gel material by using chiral SRDS based sensor is realized in this part of the study as a density sensor. Sensor layer with a thickness of $g_i = 0.76$ mm is filled with calcium chloride material of which relative dielectric constant ε_i depends on density. Dielectric constant changes of Calcium chloride according to its density are given in [31] between 8 GHz–12 GHz. The numerical data are seen in the inset of Fig. 8. Complex permittivity of Calcium chloride does not have any significant changes in X band frequencies. This is a real disadvantage because of the sensing problem. Since the chiral SRDS based sensor has to resonate near 10 GHz, and the resonance frequency is constant, dielectric constant of the Calcium Chloride can be accepted as it is related with the density only at around 10 GHz. The SRDS based sensor filled with calcium chloride is parametrically defined and simulated in CST Microwave Studio to evaluate resonance frequencies for different density values, and then the relations of the dielectric constant of the Calcium Chloride, density and resonance frequency are presented in Fig. 9. While the density of sandwiched calcium chloride sample between SDRS inclusions changes between 17% to 22.5%, the relative permittivity varies between 1.41 and 1.70, and the simulated resonance frequency shifts from 9.96 GHz to 9.952 GHz. The increment of the dielectric constant results in the reduction of resonance frequency due to the increment of both C_{self} and C_{mut}. The resonance frequency change is not linear with respect to the density of sandwiched calcium chloride since the main parameter, i.e., dielectric constant change does not linearly vary depending on the density. Besides, the curve represents the resonance frequency-density dependency similar to a piecewise linear curve with a slope of 9 MHz/percentage of density. This step change is much more sensible than the MTM based density sensor studies and can be used as density sensor without any drawback since it is higher than the resolution of network analyzers [32]. According to the simulation results, the angle between resonance frequency and relative density value is about 25°. Because of the slight distortion of the linearity of the resonance frequency-density curve, it can be dealt with three separated linear sections with a slop of 8 MHz/density, 16 MHz/density, 2 MHz/density for the range of 17–21, 21–21.5 and 21.5–22.5 density percentages, respectively.

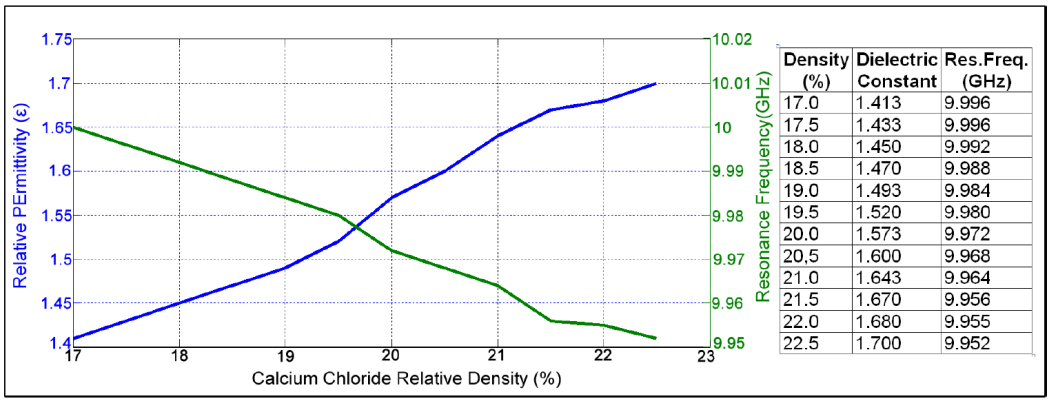

Density (%)	Dielectric Constant	Res.Freq. (GHz)
17.0	1.413	9.996
17.5	1.433	9.996
18.0	1.450	9.992
18.5	1.470	9.988
19.0	1.493	9.984
19.5	1.520	9.980
20.0	1.573	9.972
20,5	1.600	9.968
21.0	1.643	9.964
21.5	1.670	9.956
22.0	1.680	9.955
22.5	1.700	9.952

Figure 9. Effects of density in relative permittivity and resonance frequency in SRDS based sensor.

6.3. SRDS Based Temperature Sensor

In this part of the study, SRDS based chiral metamaterial structure is used as a temperature sensor for measuring temperature of a marrowbone. Sensing of marrowbone temperature is highly important for health applications. It is well known that curative properties of electromagnetic waves are investigated by observing radiated heat from biological tissues in the case of electromagnetic wave (EM) absorption. Whereas the tissues and the skin with conductivity properties absorb maximum EM energy, fat and muscles have less absorption properties. Heating properties of different biological tissues are related with liquid rates. But the absorption is directly proportional to layer numbers of any biological tissues with variable permittivity. Hence, the sensing of heat change of any biological tissue, such as marrowbone, is very important to deciding EM absorption rates.

To realize this, the sensor layer thickness is fixed to 0.76 mm, and sensor layer is assumed to be filled with marrowbone in different temperatures. In this sensing application, marrowbone's electromagnetic properties such as dielectric constant and loss tangent values are taken from [33] at the frequency of 10 GHz between 30°C–90°C. Marrowbone's complex relative permittivity changes according to its temperature. When the relative permittivity changes due to the temperature, it affects the relative permittivity of the sensor layer according to $\varepsilon_i = \varepsilon_r' - j\varepsilon_r''$. For marrowbone, dielectric constant and loss tangent values are obtained from Hippel's method around 9.5 GHz [34, 35].

$$\varepsilon' = \frac{k^2 + \beta^2 - \alpha^2}{\beta_0^2} \tan\delta = \frac{2\alpha\beta}{k^2 + \beta^2 - \alpha^2} \tag{4}$$

$$\gamma = \alpha + j\beta, \quad k = \frac{2\pi}{\lambda_c} \quad \text{and } \beta_0 = \frac{2\pi}{\lambda} \tag{5}$$

The propagation constant is evaluated from the equation of the hyperbolic tangent instead of ordinary tangent. All the other quantities are the same as for the "twice-minimum" method mentioned above [34]. SRDS based chiral sensor simulation is completed according to the complex dielectric constant data given in the inset of Fig. 10. These data are used to observe sensing of the SRDS based chiral sensor with respect to the change of the dielectric constant, in other words, temperature changes. After simulation, resonance frequency/permittivity of marrowbone versus tissue temperature changes is plotted in Fig. 10. When the temperature of the marrowbone tissue is increased from 30°C to 90°C, resonance frequency decreases from 9.54 GHz to 9.508 GHz. Resonance frequency of the SRDS based chiral sensor with respect to the temperature is also piecewise linear curve. The slope of the curve is nearly 1 MHz per temperature step, and it has observable frequency resolution for all types of network analyzer. The plot can be analyzed separately for two exact linear parts in order to obtain accurate slope of the relationship. The first linear part has a slope of 65° for unit temperature over the range of 30–50°C, and the second linear part has a slope of 40° for unit temperature over the range of 50–90°C. When we look at the overall slopes of dielectric constant and resonance frequency, they are found as 51° and 55°.

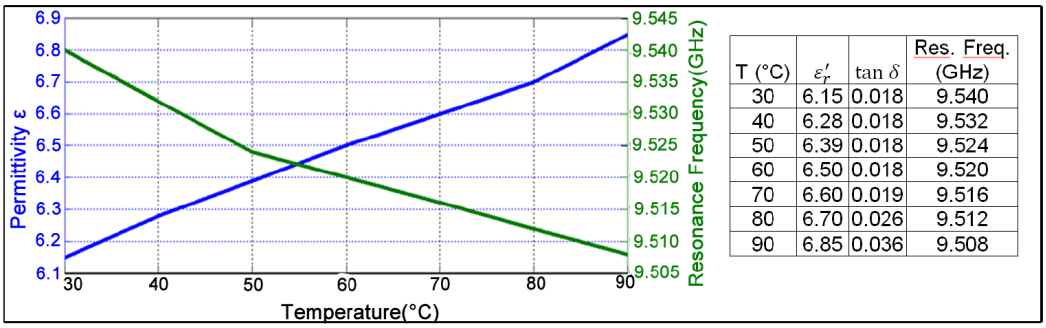

T (°C)	ε_r'	tan δ	Res. Freq. (GHz)
30	6.15	0.018	9.540
40	6.28	0.018	9.532
50	6.39	0.018	9.524
60	6.50	0.018	9.520
70	6.60	0.019	9.516
80	6.70	0.026	9.512
90	6.85	0.036	9.508

Figure 10. Variations of resonance frequency of the SRDS based sensor according to different temperatures.

7. CONCLUSION

The proposed study is focused on multifunctional chiral sensor based on SRDS as a sensing device of variable purposes such as pressure, humidity, density and temperature sensation. The sensing properties of the proposed chiral sensor design are proved both numerically and experimentally. The advantages and efficiency of the chiral sensor are exhibited for various important application purposes such as humidity sensor for sand, density sensor for calcium chloride and temperature sensor for a marrowbone. The linearity of the sensing frequency changes, and stability of the amplitude of the transmission level provides the researchers a novel sensor which is applicable to realize many different sensing applications by using a single structure, such as medical area. The chiral sensor based on SRDS inclusion can also be used for terahertz applications for future sensor studies instead of using metamaterial based sensors, especially sensing chiral structures.

There are some metamaterial-based sensing studies in literature. Unlike the literature studies related with this subject, this study has many advantages. The proposed model is presented as multi-functional such as pressure, humidity, density and temperature sensation. In addition, it has easy fabrication techniques and materials. The suggested design uses low cost materials and has simple configuration. Moreover, the proposed sensor is based on chiral metamaterial. There is not any study in literature about the chiral metamaterial based sensor in microwave range. Besides, the stability of the transmission especially for pressure sensor will help to design adjustable sensors with varicaps at only a fixed frequency value for future studies. Due to facility capabilities, measurements regarding to humidity, temperature of biological tissue and silica gel density could not be realized. For future studies, it is planned to realize humidity, temperature and density measurement experiments.

ACKNOWLEDGMENT

Related measurements in this work is supported by Prof. Cumali Sabah. Also, authors would like to thank editors and anonymous reviewers for their valuable suggestions to improve the paper.

REFERENCES

1. Pendry, J. B., "Negative refraction makes a perfect lens," *Physical Review Letters*, Vol. 85, No. 18, 3966–3975, 2000.
2. Pendry, J. B., "Electromagnetic materials enter the negative age," *Physics World*, Vol. 14, No. 9, 47–51, 2001.
3. Yang, J. J., M. Huangand, and J. Sun, "Double negative metamaterial sensor based on micro ring resonator," *IEEE Sensor*, Vol. 11, 2254–2259, 2011.
4. Yang, J., M. Huang, Y. Lan, and Y. Li, "Microwave sensor based on a single stereo-complementary asymmetric split resonator," *International Journal of RF and Microwave Computer-aided Engineering,* Vol. 22, 545–551, 2012.

5. Schueler, M., C. Mandel, M. Puentesand, and R. Jakoby, "Metamaterial inspired microwave sensors," *IEEE Microwave Magazine*, Vol. 13, 57–68, 2012.
6. Melik, R., E. Unal, N. K. Perkgoz, B. Santoni, D. Kamstock, C. Puttlitzand, and H. V. Demir, "Nested metamaterials for wireless strain sensing," *IEEE Journal of Selected Topics in Quantum Electronics,* Vol. 16, 450–458, 2010.
7. Cheng, Y., Y. Nie, Z. Cheng, and R. Z. Gong, "Dual-band circular polarizer and linear polarization transformer based on twisted split-ring structure asymmetric chiral metamaterial," *Progress In Electromagnetics Research,* Vol. 145, 263–272, 2014.
8. Cheng, Y., Y. Nie, L. Wu, and R. Z. Gong, "Giant circular dichroism and negative refractive index of chiral metamaterial based on split-ring resonators," *Progress In Electromagnetics Research,* Vol. 138, 263–272, 2013.
9. Sonsilphong, A. and N. Wongkasem, "Three-dimensional artificial double helices with high negative refractive index," *Journal of Optics,* Vol. 14, 105103, 2012.
10. Wongkasem, N., C. Kamtongdee, A. Akyurtlu, and K. Marx, "Artificial multiple helices: Polarization and EM properties," *Journal of Optics,* Vol. 12, 075102, 2010.
11. Dincer, F., C. Sabah, M. Karaaslan, M. Bakir, and U. Erdiven, "Asymmetric transmission of linearly polarized waves and dynamically wave rotation using chiral metamaterial," *Progress In Electromagnetics Research*, Vol. 140, 227–239, 2013.
12. Sabah, C., H. T. Tastan, F. Dincer, K. Delihacioglu, M. Karaaslan, and E. Unal, "Transmission tunneling through the multilayer double-negative and double-positive slabs," *Progress In Electromagnetics Research*, Vol. 138, 293–306, 2013.
13. Ekmekci, E., R. D. Averitt, and G. T. Sayan, "Effects of substrate parameters on the resonance frequency of double-sided SRR structures under two different excitations," *PIERS Proceedings*, 538–540, Cambridge, USA, Jul. 5–8, 2010.
14. Kriegler, C., "Bianisotropic photonic metamaterials," *IEEE Journal of Selectedtopics in Quantum Electronics*, 1–15, 2010.
15. Wang, B., "Chiral metamaterials: Simulations and experiments," *Journal of Optics A, Pure and Applied Optics,* Vol. 11, No. 11, 114003–114013, 2009.
16. Tretyakov, S., A. Sihvolaand, and L. Jylhä, "Backward-wave regime and negative refraction in chiral composites," *Photonics and Nanostructures Fundamentals and Applications*, Vol. 3, Nos. 2–3, 107–115, 2005.
17. Chen, T., S. Liand, and H. Suun, "Metamaterials application in sensing," *Sensors*, Vol. 12, 2742–2765, 2012.
18. Soukoulis, C. M., S. Lindenand, and M. Wegener, "Negative refractive index at optical wavelengths," *Science*, Vol. 315, No. 5808, 47–49, 2007.
19. Aydin, K., I. Bulu, K. Guven, M. Kafesaki, C. M. Soukoulis, and E. Ozbay, "Investigation of magnetic resonances for different split-ring resonator parameters and designs," *New J. Phys.*, Vol. 7, 168–182, 2005.
20. Ekmekci, E. and G. T. Sayan, "Multi-functional metamaterial sensor based on a broad-side coupled SRR topology with a multi-layer substrate," *Applied Physics A: Materials Science & Processing*, Vol. 110, No. 1, 189–197, 2013.
21. Hendry, E., T. Carpy, J. Johnston, M. Popland, R. Mikhaylovskiy, A. J. Lapthorn, S. M. Kelly, L. D. Barron, N. Gadegaard, and M. Kadodwala, "Ultrasensitive detection and characterization of biomolecules using superchiral fields," *Nature Nanoletters*, Vol. 5, 783–787, 2010.
22. Meng, F., Q. Wu, D. Erni, K. Wu, and J. C. Lee, "Polarization-independent metamaterial analog of electromagnetically induced transparency for a refractive-index-based sensor," *IEEE Transactions on Microwave Theory and Techniques*, Vol. 60, No. 10, 3013–3022, 2012.
23. Willets, K. A. and R. P. van Duyne, "Localised surface plasmon resonance spectroscopy and sensing," *Ann. Rev. Phys. Chem.*, Vol. 58, 267–297, 2007.
24. Anker, J. N., W. Paige, O. Lyandres, C. Shah, J. Zhao, and R. V. Duyne, "Bio sensing with plasmonic nanosensors," *Nature Materials*, Vol. 7, 442–453, Jun. 2008.

25. Link, S. and M. A. El Sayed, "Spectral properties and relaxation dynamics of surface plasmon electronic oscillations in gold and silver nanodots and nanorods," *J. Phys. Chem. B.*, Vol. 103, 8410–8426, 1999.
26. Haes, A. J. and R. P. Duyne, "A nanoscale optical biosensor: Sensitivity and selectivity of an approach based on the localised surface plasmon resonance spectroscopy of triangular silver nanoparticles," *J. Am. Chem. Soc.*, Vol. 124, 10596–10604, 2002.
27. Jung, L. S., C. T. Campell, T. M. Chinowsky, M. N. Mar, and S. S. Yee, "Quantitative interpretation of the response of surface plasmon resonance sensors to adsorbed film," *Langmuir*, Vol. 14, 5636–5648, 1998.
28. Barbillon, G., "Plasmonic nanostructures prepared by soft UV nanoimprint lithography and their application in biological sensing," *Micromachines*, Vol. 3, 21–27, 2012.
29. Withayachumnankula, W., K. Jaruwongrungseeb, A. Tuantranontc, C. Fumeauxa, and D. Abbotta, "Metamaterial-based microfluidic sensor for dielectric characterization," *Sensors and Actuators A: Physical*, Vol. 189, 233–237, 2013.
30. Vishvakarma, R. B. and C. S. Raid, "Measurement of complex dielectric constant of sand and dust particles as a function of moisture content," *European Microwave Conference*, Vol. 23, 568–570, 1993.
31. Zheng, Y., G. Meyer, M. Lanagan, A. Dinesh, and C. Jiping, "A study of watersorption effects on the microwave dielectric properties," *Materials Letters,* Vol. 95, 157–159, 2013.
32. Yang, J., M. Huang, H. Tang, J. Zeng, and L. Dong, "Metamaterial sensors," *International Journal of Antennas and Propagation*, Vol. 2013, 637270, 2013.
33. Factorova, D., "Temperature dependence of biological tissues complex permittivity at microwave frequencies," *Advances in Electrical and Electronic Engineering*, Vol. 7, 354–357, 2008.
34. Baker, J., E. Vanzura, and W. Kissik, "Improved technique for determining complex permittivity with the transmission/reflection method," *IEEE Transactions on Microwave Theory and Techniques*, Vol. 38, 1096–1103, 1990.
35. Faktorová, D., "Microwave nondestructive testing of dielectric materials," *Advances in Electrical and Electronic Engineering*, Vol. 5, 230–233, 2006.